

AperTO - Archivio Istituzionale Open Access dell'Università di Torino

Chemical inhibition of xylem cellular activity impedes the removal of drought-induced embolisms in poplar stems – new insights from micro-CT analysis

This is a pre print version of the following article:

Original Citation:

Availability:

This version is available <http://hdl.handle.net/2318/1765649> since 2021-10-22T13:27:45Z

Published version:

DOI:10.1111/nph.16912

Terms of use:

Open Access

Anyone can freely access the full text of works made available as "Open Access". Works made available under a Creative Commons license can be used according to the terms and conditions of said license. Use of all other works requires consent of the right holder (author or publisher) if not exempted from copyright protection by the applicable law.

(Article begins on next page)

1 **X-ray micro CT analyses of embolism formation and impact of cellular activity on xylem**
2 **recovery from stress in poplar trees**

3

4 Francesca Secchi¹, Chiara Pagliarani², Silvia Cavalletto¹, Francesco Petruzzellis³, Giulia Tonel¹,
5 Tadeia Savi³, Giuliana Tromba⁴, Maria Margherita Obertino¹, Claudio Lovisolò¹, Andrea
6 Nardini³, Maciej A. Zwieniecki⁵

7

8 ¹) Department of Agriculture, Forest and Food Sciences, University of Turin, Largo Paolo
9 Braccini 2, 10095 Grugliasco, Italy

10 ²) Institute for Sustainable Plant Protection, National Research Council, Strada delle Cacce 73,
11 Torino, Italy

12 ³) Dipartimento di Scienze della Vita, University of Trieste, via Giorgieri 10, 34127 Trieste
13 (Italy)

14 ⁴) Elettra-Sincrotrone Trieste, Area Science Park, 34149 Basovizza, Trieste, Italy

15 ⁵) Department of Plant Sciences, University of California Davis, One Shields Avenue, 95616
16 Davis (CA), USA

17

18 Author for correspondence:

19 *Francesca Secchi*

20 Tel: +39 011 6708655

21 Email: francesca.secchi@unito.it

22

Total word count (excluding summary, references and legends):		No. of figures:	6
Summary:		No of Tables:	0
Introduction:		No. of Supporting Information files:	1 (Fig. S1)
Material and Methods:			
Results:			
Discussion and Conclusion:			
Acknowledgements			

23

24

25 **Summary**

26 In drought stressed plants a coordinated cascade of chemical and transcriptional adjustments
27 occurs concurrently to embolism formation. While these processes do not affect embolism
28 formation during stress, they may prime stems for recovery during rehydration by modifying
29 apoplast pH and increasing sugar concentration in the xylem sap.

30 Here we show that *in vivo* treatments modifying apoplastic pH (stem infiltration with a pH
31 buffer) or reducing stem metabolic activity (infiltration with sodium vanadate and sodium
32 cyanide; plant exposure to carbon monoxide) can reduce sugar accumulation, thus disrupting or
33 delaying the recovery process.

34 Application of the vanadate treatment (NaVO_3 , an inhibitor of many ATP-ases) completely
35 halted recovery from drought-induced embolism for up to 24 hours after re-irrigation, while
36 partial recovery was observed *in vivo* in control plants using X-ray micro-CT.

37 Our results suggest that stem hydraulic recovery in poplar is a biological, energy dependent
38 process that coincides with accumulation of sugars in the apoplast during stress. Recovery and
39 damage are spatially coordinated, with embolism formation occurring from the inside-out and
40 refilling from the outside-in. The outside-in pattern highlights the importance of xylem proximity
41 to the sugars within the phloem to the embolism recovery process.

42

43 Key words: apoplastic pH, embolism, *Populus*, recovery, sugars, X-ray micro-computed
44 tomography (micro-CT), vanadate, xylem

45

46 **Introduction**

47 Survival of vascular plants under drought is intimately linked to maintaining the
48 functionality of their xylem network. While physical aspects of long-distance water transport in
49 vascular plants and formation/spread of embolism are well understood (Stroock *et al.*, 2014;
50 Jensen *et al.*, 2016), the biology of active recovery from embolism remains hotly debated
51 (Nardini *et al.*, 2011; Brodersen & McElrone, 2013; Knipfer *et al.*, 2016). Groups of researchers
52 think that, in some species, no embolism recovery occurs under natural conditions (Charrier *et al.*,
53 2016; Lamarque *et al.*, 2018; Choat *et al.*, 2019) while others assert that recovery is a
54 common process that can take place even under moderate xylem tensions (Salleo *et al.*, 2009;
55 Zwieniecki & Holbrook, 2009; Brodersen *et al.*, 2010; Secchi & Zwieniecki, 2011; Tomasella *et al.*,
56 2019a). Major controversies originate from the fact that the most of the techniques used to
57 study plant hydraulic properties are destructive, and with doubted reliability (Cochard *et al.*,
58 2013). Some techniques could indeed cause artefacts (e.g. increased percent loss of conductivity
59 (PLC) values) due to the excision of xylem under tension, thus potentially allowing for spurious
60 air entry into the conduits even if stems were cut under water (Wheeler *et al.*, 2013). Other
61 techniques can cause supersaturation with positive air pressure that could induce embolism and
62 the appearance of its rapid recovery. However, the presence and significance of these artefacts
63 are questioned (Trifilo *et al.*, 2014; Fukuda *et al.*, 2015; Scoffoni & Sack, 2015; Ogasa *et al.*,
64 2016; Nardini *et al.*, 2017; Nolf *et al.*, 2017).

65 Classical hydraulic techniques for monitoring the presence of xylem embolism are
66 complemented with *in-vivo*, non-destructive techniques like magnetic resonance imaging (MRI)
67 (Holbrook *et al.*, 2001; Clearwater & Goldstein, 2005; Wang *et al.*, 2013; Zwieniecki *et al.*,
68 2013) and X-ray computed micro-tomography (X-ray micro-CT; Brodersen *et al.*, 2010;
69 McElrone *et al.*, 2013; Choat *et al.*, 2016). These contemporary techniques make it possible to
70 observe, in real time, the spatial and temporal patterns of embolism occurrence in the hydraulic
71 systems of living plants. The MRI, while very safe for living cells and capable of fast, repetitive
72 imaging, has relatively low resolution ($>20\ \mu\text{m}$) and physical limitations on fitting the stem
73 through the core of the magnet. X-ray micro-CT has emerged as the preferred technique for
74 studying xylem embolism formation (Cochard *et al.*, 2015) and its potential recovery (Brodersen
75 *et al.*, 2010; Rolland *et al.*, 2015; Brodersen *et al.*, 2018). X-ray micro-CT provides good

76 contrast between air-filled and water-filled conduits, high spatial and temporal resolution (~1
77 μm) and high signal-to-noise ratio. However, a recent study challenged the usefulness of X-ray
78 micro-CT for repeated observations of water content in the same xylem conduits due to the
79 severe damage caused to living cells by consecutive scans (Petruzzellis *et al.*, 2018). Limiting
80 xylem exposure to single scans, and reliance on observations of multiple stems, might be
81 required to confidently study the hydraulic recovery processes.

82 Despite these technical difficulties, a growing consensus suggests, that while embolism
83 formation cannot be avoided during severe water stress, recovery might be possible upon relief
84 of stress (lowering tension) and strongly reduced transpiration (Brodersen & McElrone, 2013).
85 To account for this process, several recovery models were proposed (Salleo *et al.*, 2004;
86 Zwieniecki & Holbrook, 2009; Nardini *et al.*, 2011; Brodersen & McElrone, 2013; Secchi &
87 Zwieniecki, 2016; Pagliarani *et al.*, 2019), suggesting that the living parenchyma cells associated
88 with xylem (vascular associated cells - VACs) are directly involved in supplying the water,
89 energy and osmotica needed to repair embolized vessels. During drought, soluble sugar content
90 (mostly sucrose) is proposed to increase in VACs due to elevated starch degradation rates and
91 the necessity of lowering cell osmotic potential in the xylem (Salleo *et al.*, 2009; Secchi &
92 Zwieniecki, 2011; Secchi & Zwieniecki, 2016). Increased sugar levels in VACs trigger sucrose
93 efflux to the apoplast via sucrose transporters. Local levels of sugar might be supplemented by
94 sugars supplied from the phloem, decreasing reliance on locally stored starch (Nardini *et al.*,
95 2011). Sugars and ions accumulated in the apoplast can generate up to ~ 0.2 MPa osmotic
96 pressure in non-functional vessels (Secchi & Zwieniecki, 2012), and thus build-up an osmotic
97 gradient that allows for cell-by-cell refilling against low tension (Zwieniecki & Holbrook, 2009).
98 *In vivo* observations from both MRI and X-ray micro-CT studies confirm that water may return
99 to empty vessels if a significant reduction in stress occurred (Holbrook *et al.*, 2001; Scheenen *et*
100 *al.*, 2007; Zwieniecki *et al.*, 2013; Brodersen *et al.*, 2018), and that water droplets preferentially
101 form and grow on the vessel walls that are in contact with VACs (Brodersen *et al.*, 2010).

102 The efflux of sugars is induced by low apoplastic pH conditions that promote the activity
103 of acidic invertases. In a low pH environment, acidic invertases splice sucrose to glucose and
104 fructose, thus reducing the concentration of extracellular sucrose and generating a sucrose
105 gradient between VACs and the apoplast, promoting further sucrose efflux from parenchyma.
106 Simultaneously, acidic invertase activity results in the accumulation of monosaccharides in

107 xylem sap, doubling the osmotic potential contributed by sucrose. Active pH adjustment has
108 been confirmed in poplar, where, as predicted by theoretical models, drought induces a pH
109 decrease in the apoplast, causing sugar accumulation in the xylem (Secchi & Zwieniecki, 2016).
110 These stress-related physiological activities are closely coupled to upregulation of gene
111 expressions involved in starch digestion, maltase and sucrose transport and acidic invertases
112 (Pagliarani *et al.*, 2019). All of these observed physiological and transcriptional events are
113 consistent with the priming of xylem for the recovery process. Still required to settle the
114 embolism debate, are *in vivo* observations of xylem embolism and recovery, paired with
115 experimental perturbation of xylem chemistry.

116 Although successful hydraulic recovery necessitates the activity of living parenchyma
117 cells near the xylem, the direct involvement of VACs in this process has not been demonstrated.
118 To verify VAC involvement, we perturbed stem biological activity while concurrently
119 visualizing the hydraulic recovery process. We hypothesized that, if sap acidification represents a
120 symptom/signal of severe water stress and if pH-driven sugar accumulation primes stems for
121 embolism recovery when stress is relieved, then inhibition of the biological activity of
122 parenchyma cells during stress will limit, or entirely halt, the hydraulic recovery processes. To
123 test this hypothesis, we used X-ray micro-CT observations of poplar stems under stress and post-
124 rehydration in combination with treatments inhibiting the metabolic activity of VACs. Our
125 findings reveal that: a) poplar trees can reduce embolism extent following water stress relief; b)
126 embolism formation and disappearance are spatially coordinated, with embolisms accumulating
127 from the inside-out, and recovery occurring from the outside-in, c) experimental reduction of the
128 metabolic activity of dehydrated plants significantly impedes the removal of drought-induced
129 embolisms.

130

131 **Material and Methods**

132

133 *Plant material and growth conditions*

134 Four month-old hybrid poplars (*Populus tremula* x *Populus alba* clone 717-1B4) were initially
135 grown in a greenhouse at the University of Turin under partially controlled climatic conditions.
136 The greenhouse air temperature and relative humidity averaged 22°C and 55% respectively.
137 Maximum photosynthetic photon flux density (PPFD) ranged between 1200 and 1400 μmol

138 photons $\text{m}^{-2} \text{s}^{-1}$ and 12-h-light/12-h-dark cycles were followed using halogen lamps when
139 necessary, to supplement light and guarantee a minimum PPFD of 500-600 $\mu\text{mol photons m}^{-2}$
140 s^{-1} . Each plant grew in a 2 L pot filled with a substrate composed of sandy-loam soil, expanded
141 clay, and peat (2:1:1 by weight). The experiment was conducted on 67 total poplars, ~50 cm tall
142 with a stem diameter of 3 to 4 mm. One sub-group of poplars (35 plants) was maintained in the
143 greenhouse at University of Turin, these poplars were used for the chemical manipulations and
144 preliminary analysis of xylem sap. This approach allowed us to determine the timeline of each
145 treatment to optimize time-frame selection for direct X-ray micro-CT observations. A second
146 subset of poplars (32 plants) was moved ahead of the *in vivo* experiment to the greenhouse at the
147 University of Trieste to allow three weeks of acclimation prior to the experiments conducted at
148 the Elettra Sincrotrone Trieste facility.

149

150 *Experimental design*

151 *(1) Chemical manipulations (at University of Turin)*

152 35 plants were used in this study. Five plants were kept as controls (*CTR*) and watered every
153 day to field capacity. The remaining 30 plants were gradually subjected to water stress (*WS*)
154 by reducing irrigation until the stem water potential (Ψ_{stem}) was below -1.8 MPa, a value
155 corresponding to at least 50 % of PLC (Secchi & Zwieniecki, 2014). Once the target water-
156 stress level was reached, xylem sap was collected from five plants (*stressed, not treated*);
157 using a destructive method (Secchi & Zwieniecki, 2012), the other five stressed poplars were
158 re-watered and allowed to recover over the period of 24 hours (*recovered, not treated*). After
159 one day of stress relief, xylem sap was collected. Before the re-watering phase, the
160 remaining 20 water stressed poplars were subjected to different chemical manipulations (five
161 plants for each of four treatments) to inhibit the metabolic activity of wood parenchyma cells
162 (Fig. 1a). Four different manipulations were applied:

163 a) Stem infiltration with distilled water plus sodium orthovanadate (NaVO_3 , BioLabs, New
164 England, MA), a general inhibitor of many plasma membrane proton pumps, expected to
165 reduce changes in apoplastic pH. The vanadate solution was used at a concentration of 10
166 mM.

167 b) Stem infiltration with distilled water plus sodium cyanide (NaCN, Sigma), to block
168 respiration and consequently, ATP-ase activity. The NaCN solution was used at a
169 concentration of 1.0 mM.

170 c) Stem infiltration with pH 6.5 buffer solution (100mL of 0.1 M Potassium dihydrogen
171 phosphate, 27.8 ml of 0.1M Sodium hydroxide, 72.2 ml of distilled water), for directly
172 altering apoplastic pH.

173 d) whole plant exposure to carbon monoxide (CO) gas, for impairing the oxidative
174 respiration and, consequently, ATP-ase activity.

175 For stem infiltration, 2-3 fully expanded leaves, at around 1/3 tree height, were cut-off
176 leaving petiole attached to the stem. Then a 2.5 cm-long silicon rubber tubing was attached at
177 the remaining petioles and filled with 200 μ l of solution (see Fig. **1b**). Solutions were
178 allowed to infiltrate the stem via natural stem suction for two hours. If the absorbed volume
179 exceeded the volume of the solution in the tube, additional liquid was added; on average a
180 total of \sim 0.75 ml of solution was absorbed into vascular system of each treated plant. Treated
181 plants were allowed 1-day for acclimation, then re-watered and allowed 24 hours of recovery
182 time (*recovered, treated*) before xylem sap collected for chemical analyses.

183 During the carbon monoxide treatment, poplar trees were placed in transparent plastic bags
184 (Fig. **1c**). Bags were initially deflated and later filled with CO applied thorough a silicon tube
185 connected to a CO tank until the plastic bag was fully inflated. For the next 3 hours, the
186 plants were maintained isolated in the CO-filled bags. After bag removal, treated plants were
187 allowed 1 day of acclimation, then re-watered and allowed 24 hours of recovery time
188 (*recovered, treated*) before xylem sap was extracted.

189 (2) *Plant preparation for X-ray micro-CT observation (at University of Trieste)*

190 The part 32 plants used for this part of the study, were further divided into two groups; 16
191 poplars (OV group) to be treated with a sodium ortho-vanadate solution as described above,
192 while the 16 plants belonging to the control group were left untreated. In each group, 4 plants
193 were kept as unstressed control and watered every day. The remaining 12 plants were
194 subjected to water stress ($<$ -1.8 MPa). After plants reach the target water-stress level, the OV
195 group was treated (as described for Turin experiment). Eight plants from both the control and
196 OV groups were then re-watered. X-ray micro-CT observations were performed on all

197 control, stressed, and recovered plants (four hours, until 24 hours of recovery time, with only
198 one scan per plant) at Elettra Sincrotrone Trieste, using the SYRMEP beamline
199 (www.elettra.trieste.it), (see below for specifics of X-ray, micro-CT observations)

200

201 *Measurements of stem water potential*

202 Stem water potential was measured for each plant on equilibrated non-transpiring (bagged)
203 leaves. Mature leaves were covered with aluminum foil and placed in a humidified plastic bag
204 for at least 30 minutes before excision. After excision, leaves were allowed to equilibrate for
205 more than 20 minutes in dark conditions before measuring water potential with a Scholander-
206 type pressure chamber in Turin (Soil Moisture Equipment Corp., Santa Barbara, CA, USA) and
207 with a portable pressure chamber (3005 Plant Water Status Console, Soilmoisture Equipment
208 Corp., Goleta, CA, USA) in Trieste. Stem xylem-pressure changes were monitored for the
209 duration of the experiments, from the beginning of the stress treatment until full recovery with
210 varying frequency days (drying) to hours (recovery).

211

212 *Sap sampling procedure*

213 Xylem sap from functional vessels was collected from control, stressed, recovered treated and
214 not treated plants (method in Secchi & Zwieniecki, 2012). Sap samples were kept at -20°C until
215 analyses were conducted.

216

217 *Soluble carbohydrate content and pH measurements*

218 The anthrone-sulfuric acid assay (Leyva *et al.*, 2008) was used to quantify soluble carbohydrate
219 content in xylem sap liquids. The anthrone reagent was prepared immediately before analysis by
220 dissolving 0.1 g of anthrone (0.1%) in 100 mL of concentrated sulfuric acid (98%). Standard
221 solutions were prepared by diluting a Glucose Standard Solution (1.0 mg/ml; Sigma, Saint Louis,
222 Missouri, USA). We added, 150 µl of anthrone reagent to each well of the microplate containing
223 50 µL of standard solutions, positive control (water), sample solutions, and a blank. Plates were
224 kept for 10 min at 4 °C, then incubated for 20 min at 100 °C. After heating, plates were cooled
225 down for 20 min at room temperature before absorbance at 620 nm was read with a microplate
226 reader (Multiscan Thermo Scientific). Colorimetric response was compared to the glucose

227 standard curve (0, 0.01, 0.03, 0.1, and 0.3 mg L⁻¹ glucose) and total carbohydrate content was
228 calculated as mg/mL of glucose.

229 The pH measurements were taken on sap samples using a micro pH electrode (PerpHect®
230 ROSS®, Thermo Fischer Scientific, Waltham, MA USA).

231

232 *X-ray Micro-CT observations*

233 Potted poplars were transported to the beamline (see above). Prior to X-ray micro-CT
234 observations, stem water potential was measured on each plant. To reduce sample movement
235 during scan rotation, the whole plant was wrapped in plastic film and secured to a wood skewer;
236 the pot was then fixed to the beamline sample holder such that stem distance was 10 cm from the
237 detector. The stem was scanned at about 4 cm above the root collar. Two silicon filters (0.5 mm
238 each) were used to obtain an average X-ray source energy of 25 keV, resulting in an entrance
239 dose rate in water of 47 mGy s⁻¹. X-ray window was 4 mm in height with horizontal opening up
240 to 120 mm. The exposure time was set at 100 ms, at an angular step of 2° resulting in a 3 min-
241 long scan. During the 360° rotation of the sample, a total of 1600 images were acquired (see
242 Petruzzellis *et al.*, 2018). In total 32 plants were scanned and each plant was subjected to only
243 one exposure. After the scan, 14 stems were air-cut a few mm below the scanned section to
244 induce the maximum artificial embolism. Only these samples were then re-scanned and analyzed
245 as the others, providing an additional normalization standard for PLC calculations.

246 In total, 1600 slices per sample with a spatial resolution of 2 µm were reconstructed using the
247 software SYRMEP TomoProject (Brun *et al.*, 2015) and one micro-CT slice per sample was
248 analyzed with the Image J (1.46r, NIH, <https://imagej.nih.gov>) software. For each sample, the
249 transverse area of all gas-filled (dark grey) and water-filled (light grey) xylem conduits, the total
250 area of xylem and the distance from embolized vessels to cambium were measured.

251 The average diameter of each conduit (derived from its area, and assuming a circular shape) was
252 used to calculate the theoretical hydraulic conductivity (Kt) of the xylem, using the Hagen-
253 Poiseuille equation (Tyree & Zimmermann, 2002). The sum of gas-filled (Kt_{gas}) and water-filled
254 (Kt_{water}) vessel conductivities provided total xylem conductivity (Kt_{max}). The theoretical PLC
255 was then calculated as (Kt_{gas}/ Kt_{max}) x 100.

256

257 *Statistical analyses*

258 Significant differences among treatments were tested by one-way analysis of variance
259 (ANOVA). The Fisher LSD post-hoc test was used for separating means when ANOVA results
260 were significant ($P < 0.05$). Pairwise differences between treatment means were compared with
261 Student's *t*-test. The SPSS statistical software package (v24.0, SPSS Inc., Cary, NC, USA) and
262 Sigma Plot software (Systat software Inc., San Jose, USA) were used to run the statistical
263 analyses reported above and to create figures, respectively.

264

265 **Results**

266 X-ray micro-CT observations of xylem in intact poplar plants allowed us to distinguish water-
267 filled (functional) and gas-filled (non-functional) vessels (Fig. 2a). Almost all vessels in non-
268 stressed plants (stem water potential in the range of 0 to -0.5 MPa) were water-filled (Fig. 2b-2).
269 Any higher level of stress (water potential < -0.5 MPa) was associated with an increase of gas-
270 filled conduits number (Fig. 2a and 2b-3). The calculated theoretical conductance of water
271 filled vessels vs. the conductance of all vessels was used to generate a vulnerability curve
272 (percent loss of conductivity (PLC) versus xylem pressure) and data were fitted to a four-
273 parameter, dose-response logistic curve (Fig. 2a, grey circles and grey lines). While the shape of
274 the obtained curve was similar to typical PLC curves, maximum PLC for severely stressed plants
275 only reached ~50% (Fig. 2a, red circles), a value lower than that reported previously (Secchi &
276 Zwieniecki, 2014). However, when maximum conductance was determined using only
277 functional vessels (the ones that embolized after cutting in air), the recalculated PLC matched the
278 previous hydraulic measurements (Fig. 2a – black circles and blue lines). When subtracting the
279 baseline PLC value to account for native embolisms, the Ψ_{stem} inducing 50% of PLC (P50) was
280 not statistically different between two estimates from this study (unadjusted EC50: -1.6 MPa,
281 grey line; and recalculated PLC: -1.58 MPa, Fig. 2a blue line) and P50 (-1.75 MPa; Fig. 2a red
282 circles) reported in the previous study (Secchi & Zwieniecki, 2014).

283 To facilitate current and future analysis of X-ray micro-CT scans for estimation of
284 embolism extent, we tested the correlation between calculated PLC, determined from the
285 diameters of all vessels (see material and methods) with simple measurements of the total area of
286 embolized vessels (AEV), to total area of mature xylem (AMX; Fig. 3 inset). The correlation was

287 linear with $R^2=0.97$ ($N=14$, $p<0.0001$) allowing for simplified analysis of embolism formation
288 (Fig. **1S**). Changes in embolism extent using the AEV/AMX ratio ranged from ~ 0 in non-
289 stressed plants to $7.72\% \pm 1.35$ in stressed poplars, with a ψ_{stem} of -2.32 ± 0.21 MPa, and an
290 EC50 of ~ -1.92 MPa (we used EC50 to describe a 50% change over the range of observed
291 values, not a true change in conductivity) when fitted with a four-parameter logistic curve (black
292 circles, Fig. **3a**). Embolism extent in plants that underwent water-stress treatments to levels
293 below -2.0 MPa, and were subsequently re-watered and allowed to recover for several hours
294 ($\psi_{\text{stem}} -0.93 \pm 0.18$ MPa) was $2.92\% \pm 0.14$, significantly lower than the extent determined for
295 stressed plants that did not recover ($p<0.0001$; Fig. **3a**). This reduction in the AEV:AMX ratio
296 suggests that plants recovering from water stress have fewer embolised xylem conduits than they
297 did before re-watering. The formation of embolisms and their disappearance followed a specific
298 spatial pattern, with embolism formation beginning near the pith and extending toward the
299 cambium (i.e. inside-out). This was confirmed by analysis of the ratio between distance of the
300 closest embolized vessel to cambium (EV-to-C) in each ray parenchyma wedge to distance
301 between pith and cambium (P-to-C; Fig. **4**, black circles). In plants recovering from stress, we
302 observed a significant increase of the average ratio (EV-to-C:P-to-C), suggesting that refilling of
303 vessels occurred in opposite direction, with regions that embolized last, recovering first (outside-
304 in; Fig. **4**, white circles).

305 We used three independent approaches to experimentally manipulate the chemistry of
306 xylem sap (pH and content of soluble sugars in sap) during the recovery process. Our first
307 approach changed xylem sap pH by infiltrating stems with a pH buffer (pH 6.5), reducing the
308 activity of acidic invertases. Secondly, we reduced membrane ATP-ase transport capacity by
309 infiltrating stems with sodium orthovanadate (NaVO_3) solution to disable sucrose transporters.
310 Our third approach was to reduce respiration by infiltrating stems with sodium cyanide (NaCN)
311 solution and exposing plants to gaseous carbon monoxide (CO) to reduce the availability of
312 ATP. As a control we infiltrated stems with DI water. In all cases, and independent of the
313 treatments, plants were capable of recovering water potential to non-stress levels within 24 hours
314 of re-watering (Fig. **5a**). Only NaVO_3 and CO treatments were effective in significantly
315 increasing xylem sap pH to ~ 6.6 , while the control stress-were at pH ~ 5.9 and water infiltration
316 at pH ~ 6.2 (ANOVA one-way $p= 0.001$; Fig. **5b**). Treatments with a pH buffer or NaCN did not

317 result in significant changes of xylem sap pH, either due to their short-term effects or the plant's
318 capacity to overcome their presence. High pH values (NaVO₃, CO) resulted in low sugar
319 concentrations, while all remaining treatments and stressed plants that had low xylem sap pH had
320 a higher sugar content (Fig. 5b inset).

321 We selected the NaVO₃ treatment, for its significant impact on pH and the simplicity of
322 its *in vivo* application, to determine the impact of metabolic activity on hydraulic recovery, as
323 determined by presence of embolized vessels. Following the timeline established through our
324 greenhouse experiment, NaVO₃ solution was allowed to infiltrate the stems of non-stressed and
325 severely-stressed plants (< -2.0 MPa). Subsets of each group were scanned using X-ray micro-
326 CT. Remaining stressed plants were re-watered and allowed adequate time for rehydration (from
327 4 to 24 hours) before scanning. Each plant was scanned only once to avoid X-ray exposure
328 induced tissue damage. We did not find any impact of NaVO₃ infiltration on the AEV/AMX
329 ratio in non-stressed plants, suggesting that treatment with NaVO₃ had no effect on xylem native
330 embolism (AEV/AMX ratio = ~0.0068; Fig. 6). Similarly, there was no difference on embolism
331 extent between severely stressed non-treated, and NaVO₃-treated plants (AEV/AMX ratio =
332 respectively 0.072 ± 0.016 and 0.067 ± 0.024 ; Fig. 6). However, we found a significant effect on
333 AEV/AMX ratio between NaVO₃ treated and non-treated plants after several hours of plant
334 rehydration, with treated plants showing small non-significant level of recovery (AEV/AMX
335 ratio change from 0.067 ± 0.024 to 0.0534 ± 0.023 ; Fig. 6), while non-treated plants showed
336 substantial recovery of more than 50% of their conductive capacity (AEV/AMX ratio change
337 from 0.072 ± 0.016 to 0.029 ± 0.013 ; Fig. 6), there was no difference in recovery of stem water
338 potential (Fig. 6).

339

340 Discussion

341 Combining experimental manipulations of xylem physiochemical status and X-ray
342 micro-CT observations of living plants, we show that treatments resulting in high apoplastic pH
343 during water stress are detrimental to the accumulation of soluble sugars in xylem, significantly
344 reducing the capacity of trees to refill embolized vessels upon recovery from stress without
345 impacting the recovery of stem water potential. Our results verify that recovery of water
346 potential is a non-metabolic process, while reinforcing the idea that embolism refilling – even

347 under without water stress – requires biological activity of VACs. Direct observations of xylem
348 vessels during recovery from water stress in a high pH environment support our hypothesis that
349 restoration of xylem transport capacity requires chemical priming. The chemical priming of
350 xylem involves both drop in sap pH and the accumulation of sugars in non-functional vessels
351 (Secchi & Zwieniecki, 2012).

352 In this study, X-ray micro-CT observations were used to determine both the embolism
353 formation during the plant dehydration and the hydraulic recovery following trees re-watering.
354 These *in vivo* observations confirmed that, when low tension was restored, previously droughted
355 poplar plants recovered from stress by reducing the number of embolized vessels, and potentially
356 reducing PLC. After 4 to 24 hours poplars repair ~ 60% of previously embolized conduits. The
357 results of this partial refilling presented here are consistent with xylem hydraulic recovery
358 measured previously on poplars belonging to the same clone, showing that full restoration of
359 stem hydraulic capacity can take several days (Secchi & Zwieniecki, 2014; Pagliarani *et al.*,
360 2019). Two-dimensional analyses of X-ray micro-CT scans provided detailed information on the
361 propagation of xylem embolism during dehydration and recovery after irrigation. Initially,
362 embolism occurred in the primary xylem adjacent to the pith before spreading toward the
363 cambium in correlation with increasing tension. Similar results were reported for *Populus*
364 *tremula x alba* clone (Choat *et al.*, 2016) and for *Vitis vinifera* (Brodersen *et al.*, 2013), where
365 embolisms also form first in the vessels surrounding the pith, and with the increasing stress,
366 spread radially toward the cambium within sectors of grouped vessels, via inter-vessel
367 connections and conductive xylem relays (Brodersen *et al.*, 2013). These previous results show
368 that older vessels are more prone to low-tension embolism formation, potentially suggesting the
369 presence of some degenerative processes that can limit the length of time that vessels can
370 function under excessive tension. It could also be possible that older vessels are more susceptible
371 to embolism due to cavitation fatigue (Hacke *et al.*, 2001; Stiller and Sperry, 2002), although in
372 our experiment we did not allow plants to get stress prior to experiment. Radial embolism
373 propagation, bounded by presence of parenchyma rays, may reflect the occurrence of air seeding
374 from interior vessels toward the outer perimeter, along the path of greatest vessel-to-vessel
375 contact (Choat *et al.*, 2008).

376 While the spread of embolism is relatively well documented, much less is known about

377 the spatial dynamics of vessel refilling. We observed recovery of embolized conduits in the
378 opposite direction to their propagation, i.e. outside-in, from the cambium toward the pith.
379 Although we did not observe full recovery, the extent of refilling was consistent with expected
380 values given the post-stress stem water potential. In multiple cases, recovery resulted in a
381 decrease of the average distance between the furthest embolized vessel and the pith, thus
382 suggesting that proximity to cambium is important in providing resources (sugars, ATP and
383 potentially water) for filling embolized vessels. Numerous studies have shown that non-structural
384 sugars are crucial for maintenance of xylem hydraulic function under water stress (Trifilo *et al.*,
385 2017; Tomasella *et al.*, 2019b; Tomasella *et al.*, 2020), and especially for recovery of the
386 hydraulic capacity of the xylem after drought relief (Secchi & Zwieniecki, 2011; Pagliarani *et*
387 *al.*, 2019; Tomasella *et al.*, 2019a). Theoretical models of embolism removal try to resolve the
388 energy need (Nardini *et al.*, 2011; Secchi & Zwieniecki, 2016; Pagliarani *et al.*, 2019), by
389 proposing that, during water stress, osmotica accumulate in the apoplast in the form of sugars
390 and ions. Direct analysis of xylem sap in embolized vessels indeed supports this view, as both
391 sugars and ions accumulated in non-functional vessels can provide an adequate osmotic potential
392 gradient to drain water from parenchyma cells post-recovery (Secchi & Zwieniecki, 2012).
393 Sugars, mostly sucrose derived from starch degradation, are moved from symplast to apoplast
394 through the membrane (passively) or by a proton-coupled sucrose efflux (actively). The
395 accumulation of sugars is controlled by xylem pH, which drops during water stress. A lower pH
396 induces apoplastic sucrose hydrolysis, possibly through acidic invertase activity (Pagliarani *et*
397 *al.*, 2019), and shifts the sucrose concentration gradient thereby establishing a further efflux of
398 sucrose to apoplast. The resulting accumulation of sugar decreases apoplastic water potential,
399 pulling water into the empty vessels upon relief from drought (Salleo *et al.*, 2009; Zwieniecki &
400 Holbrook, 2009; Secchi & Zwieniecki, 2012; Secchi & Zwieniecki, 2016). Proton-coupled
401 sucrose efflux is predicted by models to be responsible for the initial increase of apoplastic
402 sucrose concentration and the decrease in pH, seen in poplar. The consequent drop in pH,
403 triggers an ion efflux from living cells that additionally contributes to apoplastic osmotic
404 concentration (Secchi & Zwieniecki, 2011; Secchi & Zwieniecki, 2012). The source of ions
405 might be related to proximity to cambium and phloem, which would be required for recycling of
406 potassium ions to maintain the capacity for this activity (Thompson/Holbrook/Zwieniecki),

407 further explaining the pattern of refilling from the outside-in.

408 *In vitro*, it has been shown that in a low-pH environment, sugars continuously
409 accumulate in the xylem apoplast, and that this carbohydrate accumulation is significantly
410 reduced in the presence of vanadate, a proton pump blocker (Secchi & Zwieniecki, 2011;
411 Secchi & Zwieniecki, 2012; Secchi & Zwieniecki, 2016). Here, we prove that, when the
412 metabolic activity of stems is decreased, the extent of recovery during rehydration is
413 significantly reduced (Fig. 6). Stem infiltration with vanadate impeded the removal of
414 embolisms formed during drought (only 20% of embolized vessels recovered after stress relief),
415 while a greater extent of embolism removal (about 60%) was observed in water-treated plants.
416 Similar results were obtained in *Laurus nobilis* L., where stems radially supplied with vanadate
417 did not recover from PLC after 20 min of rehydration to low tension (Salleo *et al.*, 2004). Here
418 we provided a relatively longer water stress relief period (4 to 24 hours), and natural light
419 conditions that encompassed night. Despite this prolonged time and a period of no transpiration,
420 embolized vessels remained non-functional when metabolic activity had been reduced with
421 vanadate. This lack of recovery is associated with high xylem pH (>6) and lower soluble sugar
422 content in xylem sap (Fig. 5), suggesting that in the absence of metabolic activity, there was no
423 priming of the stem for recovery, directly linking plant chemistry to visual observations of
424 refilling activity.

425 The vulnerability curve generated by the X ray micro-CT observations did not closely
426 match the curve based on the classical hydraulic techniques, previously performed on plants
427 belonging to the same poplar clone (Secchi & Zwieniecki, 2014). The *in vivo* observations
428 resulted in underestimation of embolism formation with a maximum of PLC around 50%. The
429 discrepancy in PLC values obtained with the two techniques could be attributed to two factors.
430 First X-ray micro-CT analyses are based on transverse bidimensional reconstructed images of a
431 small scanned segment of stems, and therefore image analysis may miss partially embolized
432 vessels, and could thereby overestimate maximum conductance (Loepfe *et al.*, 2007; Pratt &
433 Jacobsen, 2018). These nonfunctional vessels, are however, accounted for in the hydraulic
434 measurements that typically examine much longer stem segments. Conversely, it is possible that
435 these traditional measurements overestimate the conductive tissue in studied stems, as the outer
436 most layer of xylem may not, as here, show any symptoms of embolisms. The outermost xylem

437 section was also slightly higher in average pixel brightness (i.e., more dense) suggesting greater
438 hydration of this part of the stem and possibility that, despite visible vessels, the near-cambial
439 sector may be immature and not yet substantially contribute to axial transport. Underestimation
440 of embolism level, through X-ray micro-CT analysis, was observed before in *Q. robur* plants
441 (Choat *et al.*, 2016); the authors suggested the possibility that many of the cells that appeared
442 filled in the images were still living and therefore non functional in transporting water. Pratt and
443 Jacobsen (2018) reported that in grapevine and American chestnut, some vessels commonly
444 observed in the outer growth rings were not contributing to transpiration, and when the samples
445 were dehydrated with air, these vessels showed some deformation suggesting that they were not
446 yet fully lignified (Pratt & Jacobsen, 2018). In our case, the evidence that vessels located in the
447 outer layer of xylem were not involved in water transport (or were not experiencing tension)
448 were obtained experimentally by rescanning stem segments that were cut in the air few mm
449 below the scanned area and allowed to form embolism due to suction in functional vessels. No
450 vessels in the outer layer ever were found to form embolisms. When only mature vessels (the
451 ones that formed embolisms after cutting in the air) were used in the calculation of PLC, the
452 resulting PLC was almost identical to previous data obtained from hydraulic measurements (Fig
453 **2a**).

454 Our results confirm that poplar trees, after re-watering and under low tension, can recover
455 from water stress by reducing the number of embolized vessels in their stems. Further, we show
456 that refilling is an active, energy-dependent process that relies on metabolically-driven
457 acidification to accumulate sugars in the apoplast during water stress. By comparing *in vivo*
458 images (without rescanning that could damage VACs) from two groups of water-stressed plants
459 – with and without experimentally reduced metabolic activity – we can conclude that refilling is
460 a part of the life of trees, and requires further studies to fully understand how it limits stress
461 survival.

462

463 **Acknowledgements**

464 This study was made possible by Elettra Sincrotrone Trieste, which granted access to the
465 SYRMEP beamline (proposal no: 20165201). We thank the technical staff at SYRMEP for the
466 assistance during experiments. Francesca Secchi gratefully acknowledges funding from Ateneo

467 CSP/2016 Project (University of Turin). The authors wish to thank Tiziano Strano for poplar
468 maintenance and Alana Chin for critical reading and help with English editing of the manuscript.

469

470 **Author Contribution**

471 FS and MAZ planned and designed the research. FS, CP and MAZ performed the chemical
472 experiments in Turin. FS, CP, SC, FP, TS, GT, AN and MAZ were involved in micro CT
473 observations. FS, SC, GT, FP made the image reconstruction. FS, CP, SC, FP, GT, MMO, CL,
474 AN and MAZ contributed to the analysis and discussion of data. FS, MAZ and AN wrote the
475 manuscript, with contribution and revision from all other authors.

476

477 **References**

478

479 **Brodersen CR, Knipfer T, McElrone AJ. 2018.** In vivo visualization of the final stages of
480 xylem vessel refilling in grapevine (*Vitis vinifera*) stems. *New Phytologist* **217**(1): 117-
481 126.

482 **Brodersen CR, McElrone AJ. 2013.** Maintenance of xylem network transport capacity: a
483 review of embolism repair in vascular plants. *Frontiers in Plant Science* **4**.

484 **Brodersen CR, McElrone AJ, Choat B, Lee EF, Shackel KA, Matthews MA. 2013.** In Vivo
485 Visualizations of Drought-Induced Embolism Spread in *Vitis vinifera*. *Plant Physiology*
486 **161**(4): 1820-1829.

487 **Brodersen CR, McElrone AJ, Choat B, Matthews MA, Shackel KA. 2010.** The Dynamics of
488 Embolism Repair in Xylem: In Vivo Visualizations Using High-Resolution Computed
489 Tomography. *Plant Physiology* **154**(3): 1088-1095.

490 **Brun F, Pacile S, Accardo A, Kourousias G, Dreossi D, Mancini L, Tromba G, Pugliese R.**
491 **2015.** Enhanced and Flexible Software Tools for X-ray Computed Tomography at the
492 Italian Synchrotron Radiation Facility Elettra. *Fundamenta Informaticae* **141**(2-3): 233-
493 243.

494 **Charrier G, Torres-Ruiz JM, Badel E, Burlett R, Choat B, Cochard H, Delmas CEL,**
495 **Domec JC, Jansen S, King A, et al. 2016.** Evidence for Hydraulic Vulnerability

496 Segmentation and Lack of Xylem Refilling under Tension. *Plant Physiology* **172**(3):
497 1657-1668.

498 **Choat B, Badel E, Burlett R, Delzon S, Cochard H, Jansen S. 2016.** Noninvasive
499 Measurement of Vulnerability to Drought-Induced Embolism by X-Ray
500 Microtomography. *Plant Physiology* **170**(1): 273-282.

501 **Choat B, Cobb AR, Jansen S. 2008.** Structure and function of bordered pits: new discoveries
502 and impacts on whole-plant hydraulic function. *New Phytologist* **177**(3): 608-625.

503 **Choat B, Nolf M, Lopez R, Peters JMR, Carins-Murphy MR, Creek D, Brodribb TJ. 2019.**
504 Non-invasive imaging shows no evidence of embolism repair after drought in tree species
505 of two genera. *Tree Physiology* **39**(1): 113-121.

506 **Clearwater M, Goldstein G 2005.** Embolism repair and long distance transport. In: Holbrook
507 NM, Zwieniecki MA eds. *Vascular Transport in Plants*: Elsevier, 201-220.

508 **Cochard H, Badel E, Herbette S, Delzon S, Choat B, Jansen S. 2013.** Methods for measuring
509 plant vulnerability to cavitation: a critical review. *Journal of Experimental Botany*
510 **64**(15): 4779-4791.

511 **Cochard H, Delzon S, Badel E. 2015.** X-ray microtomography (micro-CT): a reference
512 technology for high-resolution quantification of xylem embolism in trees. *Plant Cell and*
513 *Environment* **38**(1): 201-206.

514 **Fukuda K, Kawaguchi D, Aihara T, Ogasa MY, Miki NH, Haishi T, Umebayashi T. 2015.**
515 Vulnerability to cavitation differs between current-year and older xylem: non-destructive
516 observation with a compact magnetic resonance imaging system of two deciduous
517 diffuse-porous species. *Plant Cell and Environment* **38**(12): 2508-2518.

518 **Holbrook NM, Ahrens ET, Burns MJ, Zwieniecki MA. 2001.** In vivo observation of
519 cavitation and embolism repair using magnetic resonance imaging. *Plant Physiology*
520 **126**(1): 27-31.

521 **Jensen KH, Berg-Sorensen K, Bruus H, Holbrook NM, Liesche J, Schulz A, Zwieniecki**
522 **MA, Bohr T. 2016.** Sap flow and sugar transport in plants. *Reviews of Modern Physics*
523 **88**(3).

524 **Knipfer T, Cuneo IF, Brodersen CR, McElrone AJ. 2016.** In Situ Visualization of the
525 Dynamics in Xylem Embolism Formation and Removal in the Absence of Root Pressure:
526 A Study on Excised Grapevine Stems. *Plant Physiology* **171**(2): 1024-1036.

527 **Lamarque LJ, Corso D, Torres-Ruiz JM, Badel E, Brodribb TJ, Burlett R, Charrier G,**
528 **Choat B, Cochard H, Gambetta GA, et al. 2018.** An inconvenient truth about xylem
529 resistance to embolism in the model species for refilling *Laurus nobilis* L. *Annals of*
530 *Forest Science* **75**(3).

531 **Leyva A, Quintana A, Sanchez M, Rodriguez EN, Cremata J, Sanchez JC. 2008.** Rapid and
532 sensitive anthrone-sulfuric acid assay in microplate format to quantify carbohydrate in
533 biopharmaceutical products: Method development and validation. *Biologicals* **36**(2): 134-
534 141.

535 **Loepfe L, Martinez-Vilalta J, Pinol J, Mencuccini M. 2007.** The relevance of xylem network
536 structure for plant hydraulic efficiency and safety. *Journal of Theoretical Biology* **247**(4):
537 788-803.

538 **McElrone AJ, Choat B, Parkinson DY, MacDowell AA, Brodersen CR. 2013.** Using High
539 Resolution Computed Tomography to Visualize the Three Dimensional Structure and
540 Function of Plant Vasculature. *Jove-Journal of Visualized Experiments*(74).

541 **Nardini A, Lo Gullo MA, Salleo S. 2011.** Refilling embolized xylem conduits: Is it a matter of
542 phloem unloading? *Plant Science* **180**(4): 604-611.

543 **Nardini A, Savi T, Losso A, Petit G, Pacile S, Tromba G, Mayr S, Trifilo P, Lo Gullo MA,**
544 **Salleo S. 2017.** X-ray microtomography observations of xylem embolism in stems of
545 *Laurus nobilis* are consistent with hydraulic measurements of percentage loss of
546 conductance. *New Phytologist* **213**(3): 1068-1075.

547 **Nolf M, Lopez R, Peters JMR, Flavel RJ, Koloadin LS, Young IM, Choat B. 2017.**
548 Visualization of xylem embolism by X-ray microtomography: a direct test against
549 hydraulic measurements. *New Phytologist* **214**(2): 890-898.

550 **Ogasa MY, Utsumi Y, Miki NH, Yazaki K, Fukuda K. 2016.** Cutting stems before relaxing
551 xylem tension induces artefacts in *Vitis coignetiae*, as evidenced by magnetic resonance
552 imaging. *Plant Cell and Environment* **39**(2): 329-337.

553 **Pagliarani C, Casolo V, Beiragi MA, Cavalletto S, Siciliano I, Schubert A, Gullino ML,**
554 **Zwieniecki MA, Secchi F. 2019.** Priming xylem for stress recovery depends on
555 coordinated activity of sugar metabolic pathways and changes in xylem sap pH. *Plant*
556 *Cell and Environment* **42**(6): 1775-1787.

557 **Petruzzellis F, Pagliarani C, Savi T, Losso A, Cavalletto S, Tromba G, Dullin C, Bar A,**
558 **Ganthaler A, Miotto A, et al. 2018.** The pitfalls of in vivo imaging techniques: evidence
559 for cellular damage caused by synchrotron X-ray computed micro-tomography. *New*
560 *Phytologist* **220**(1): 104-110.

561 **Pratt RB, Jacobsen AL. 2018.** Identifying which conduits are moving water in woody plants: a
562 new HRCT-based method. *Tree Physiology* **38**(8): 1200-1212.

563 **Rolland V, Bergstrom DM, Lenne T, Bryant G, Chen H, Wolfe J, Holbrook NM, Stanton**
564 **DE, Ball MC. 2015.** Easy Come, Easy Go: Capillary Forces Enable Rapid Refilling of
565 Embolized Primary Xylem Vessels. *Plant Physiology* **168**(4): 1636-1647.

566 **Salleo S, Lo Gullo MA, Trifilo' P, Nardini A. 2004.** New evidence for a role of vessel-
567 associated cells and phloem in the rapid xylem refilling of cavitated stems of *Laurus*
568 *nobilis* L. *Plant, Cell and Environment* **27**: 1065-1076.

569 **Salleo S, Trifilo' P, Esposito S, Nardini A, Lo Gullo MA. 2009.** Starch-to-sugar conversion in
570 wood parenchyma of field-growing *Laurus nobilis* plants: a component of the signal
571 pathway for embolism repair? *Functional Plant Biology* **36**: 815-825.

572 **Savi T, Miotto A, Petruzzellis F, Losso A, Pacile S, Tromba G, Mayr S, Nardini A. 2017.**
573 Drought-induced embolism in stems of sunflower: A comparison of in vivo micro-CT
574 observations and destructive hydraulic measurements. *Plant Physiology and*
575 *Biochemistry* **120**: 24-29.

576 **Scheenen TWJ, Vergeldt FJ, Heemskerk AM, Van As H. 2007.** Intact plant magnetic
577 resonance imaging to study dynamics in long-distance sap flow and flow-conducting
578 surface area. *Plant Physiology* **144**(2): 1157-1165.

579 **Scoffoni C, Sack L. 2015.** Are leaves 'freewheelin'? Testing for a Wheeler-type effect in leaf
580 xylem hydraulic decline. *Plant Cell and Environment* **38**(3): 534-543.

581 **Secchi F, Zwieniecki MA. 2011.** Sensing embolism in xylem vessels: the role of sucrose as a
582 trigger for refilling. *Plant, Cell and Environment* **34**(3): 514-524.

583 **Secchi F, Zwieniecki MA. 2012.** Analysis of Xylem Sap from Functional (Nonembolized) and
584 Nonfunctional (Embolized) Vessels of *Populus nigra*: Chemistry of Refilling. *Plant*
585 *Physiology* **160**(2): 955-964.

586 **Secchi F, Zwieniecki MA. 2014.** Down-Regulation of Plasma Intrinsic Protein1 Aquaporin in
587 Poplar Trees Is Detrimental to Recovery from Embolism. *Plant Physiology* **164**(4): 1789-
588 1799.

589 **Secchi F, Zwieniecki MA. 2016.** Accumulation of sugars in the xylem apoplast observed under
590 water stress conditions is controlled by xylem pH. *Plant Cell and Environment* **39**(11):
591 2350-2360.

592 **Stroock AD, Pagay VV, Zwieniecki MA, Holbrook NM 2014.** The Physicochemical
593 Hydrodynamics of Vascular Plants. In: Davis SH, Moin P eds. *Annual Review of Fluid*
594 *Mechanics, Vol 46*, 615-642.

595 **Tomasella M, Casolo V, Aichner N, Petruzzellis F, Savi T, Trifilo P, Nardini A. 2019a.** Non-
596 structural carbohydrate and hydraulic dynamics during drought and recovery in *Fraxinus*
597 *ornus* and *Ostrya carpinifolia* saplings. *Plant Physiology and Biochemistry* **145**: 1-9.

598 **Tomasella M, Nardini A, Hesse BD, Machlet A, Matyssek R, Haberle KH. 2019b.** Close to
599 the edge: effects of repeated severe drought on stem hydraulics and non-structural
600 carbohydrates in European beech saplings. *Tree Physiology* **39**(5): 717-728.

601 **Tomasella M, Petrusa E, Petruzzellis F, Nardini A, Casolo V. 2020.** The Possible Role of
602 Non-Structural Carbohydrates in the Regulation of Tree Hydraulics. *International*
603 *Journal of Molecular Sciences* **21**(1).

604 **Trifilo P, Casolo V, Raimondo F, Petrusa E, Boscutti F, Lo Gullo MA, Nardini A. 2017.**
605 Effects of prolonged drought on stem non-structural carbohydrates content and post-
606 drought hydraulic recovery in *Laurus nobilis* L.: The possible link between carbon
607 starvation and hydraulic failure. *Plant Physiology and Biochemistry* **120**: 232-241.

608 **Trifilo P, Raimondo F, Lo Gullo MA, Barbera PM, Salleo S, Nardini A. 2014.** Relax and
609 refill: xylem rehydration prior to hydraulic measurements favours embolism repair in
610 stems and generates artificially low PLC values. *Plant Cell and Environment* **37**(11):
611 2491-2499.

612 **Tyree MT, Zimmermann MH. 2002.** *Xylem Structure and the Ascent of Sap*. New York:
613 Springer-Verlag.

614 **Wang MT, Tyree MT, Wasylshen RE. 2013.** Magnetic resonance imaging of water ascent in
615 embolized xylem vessels of grapevine stem segments. *Canadian Journal of Plant Science*
616 **93(5): 879-893.**

617 **Wheeler JK, Huggett BA, Tofte AN, Rockwell FE, Holbrook NM. 2013.** Cutting xylem under
618 tension or supersaturated with gas can generate PLC and the appearance of rapid
619 recovery from embolism. *Plant Cell and Environment* **36(11): 1938-1949.**

620 **Zwieniecki MA, Holbrook NM. 2009.** Confronting Maxwell's demon: biophysics of xylem
621 embolism repair. *Trends in Plant Science* **14(10): 530-534.**

622 **Zwieniecki MA, Melcher PJ, Ahrens ET. 2013.** Analysis of spatial and temporal dynamics of
623 xylem refilling in *Acer rubrum* L. using magnetic resonance imaging. *Frontiers Plant*
624 *Science* **4: 265.**

625

626

627 **Figure legends**

628

629 **Fig. 1** (a) Schematic representation of experimental set-up. (b) Stem infiltration with sodium
630 ortho-vanadate solution. (c) Plant exposure to carbon monoxide.

631

632 **Fig. 2** (a) Vulnerability curves for *Populus alba x tremula* plants based on: xylem theoretical
633 hydraulic conductivity of plants subjected to one x-ray exposure (grey circles-lines); xylem
634 theoretical hydraulic conductivity normalized with data obtained by stems first air-cut (to induce
635 maximum artificial embolism formation) and then re-scanned (black circles and blue lines);
636 hydraulic measurements previously performed on the same poplar clone (red circles, Secchi and
637 Zwieniecki 2014). Each circle corresponds to a plant. (b) *In vivo* visualization by X-ray
638 microtomography of xylem emboli in stems of *Populus tremula x alba* intact plants.
639 Reconstructed cross sections showing gas-filled (dark grey) and water-filled (light grey) xylem
640 conduits during well watered and stress conditions. 1-2 cross-sections of stressed and control
641 stems scanned once and the same stems exposed to a second exposure after air-cutting (3-4).

642

643 **Fig. 3** (a) Percent of total area of embolized vessels (AEV) on total area of mature xylem (AMX)
644 in response to changes in xylem pressure during drought and recovery treatments. Data were
645 fitted with a four-parameter logistic curve (dose-response curve); each circle corresponds to a
646 plant. (b) *In vivo* visualization by X- ray microtomography (micro-CT) in stems of intact
647 *Populus tremula x alba* plants. Reconstructed cross-sections showing embolized (air-filled
648 vessels, dark circles) and functional conduits (water-filled, light grey circles) in stressed,
649 recovered, and well-watered plants, respectively.

650

651 **Fig. 4** Ratio between the distance of the closest embolized vessels to cambium (EV-to-C) in each
652 ray parenchyma wedge to the distance between the pith and cambium (P-to-C) in stressed, well-
653 watered, and recovered plants. Circles are mean values of multiple embolized vessels belonging
654 to a single plant and error bars represent SD. Inset: Reconstructed cross section showing distance
655 from pith to the cambium (yellow lines) and from the closest embolized vessels to cambium (red
656 dotted lines).

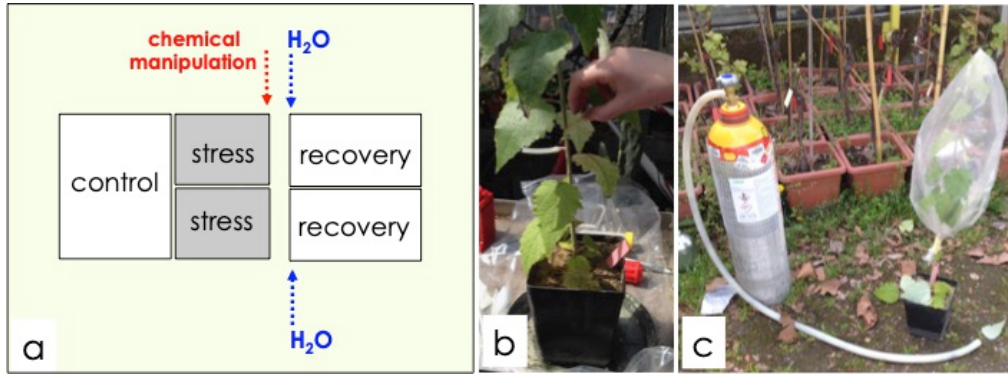
657 **Fig. 5** Effect of chemical treatments (sodium orthovanadate, NaVO_3 ; carbon monoxide, CO ;
658 pH6.5 buffer solution and sodium cyanide, NaCN) on: (a) Xylem pressure measured on non-
659 transpiring leaves (Ψ_{stem}). and (b) xylem pH. Inset: average xylem sugar content measured for
660 each treatment as it relates to average pH values. All plants were water-stressed and then
661 chemically treated, allowing for 1 day for acclimation. Poplars were re-watered, and after 24
662 hours of recovery, xylem sap was collected. One-way ANOVA test suggests significant
663 differences in xylem pressure ($p < 0.001$), pH values ($p = 0.001$) and sugar content ($p < 0.001$)
664 between different chemical treatments in plants recovering from stress. Letters denote
665 homogeneous groups based on the Fisher LSD method; bars are mean values, and error bars
666 represent SE.

667

668 **Fig. 6** Percentage of total area of embolized vessels (AEV) on total area of mature xylem (AMX)
669 in response to xylem pressure for non treated plants (black circles) and for poplar that before the
670 recovery phase were chemical treated with a solution 10 mM of sodium orthovanadate (light
671 grey squares). Symbols are mean values of multiple embolized vessels belonging to a single
672 plant and error bars represent SD. Asterisk denotes significant differences between treated and
673 non-treated, recovering plants, tested using a t-test ($p < 0.05$).

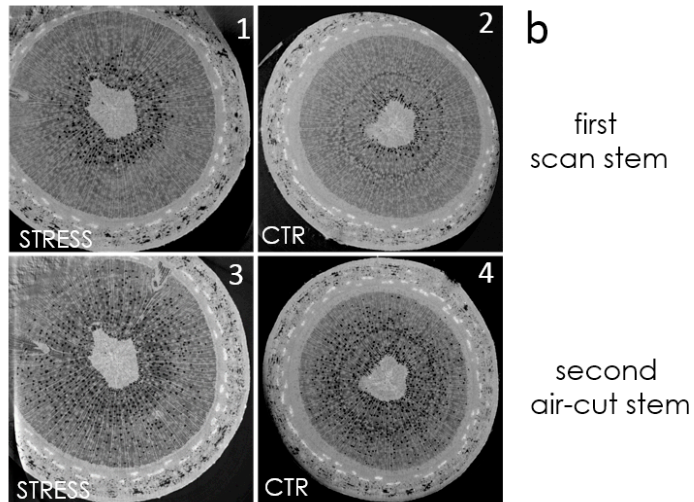
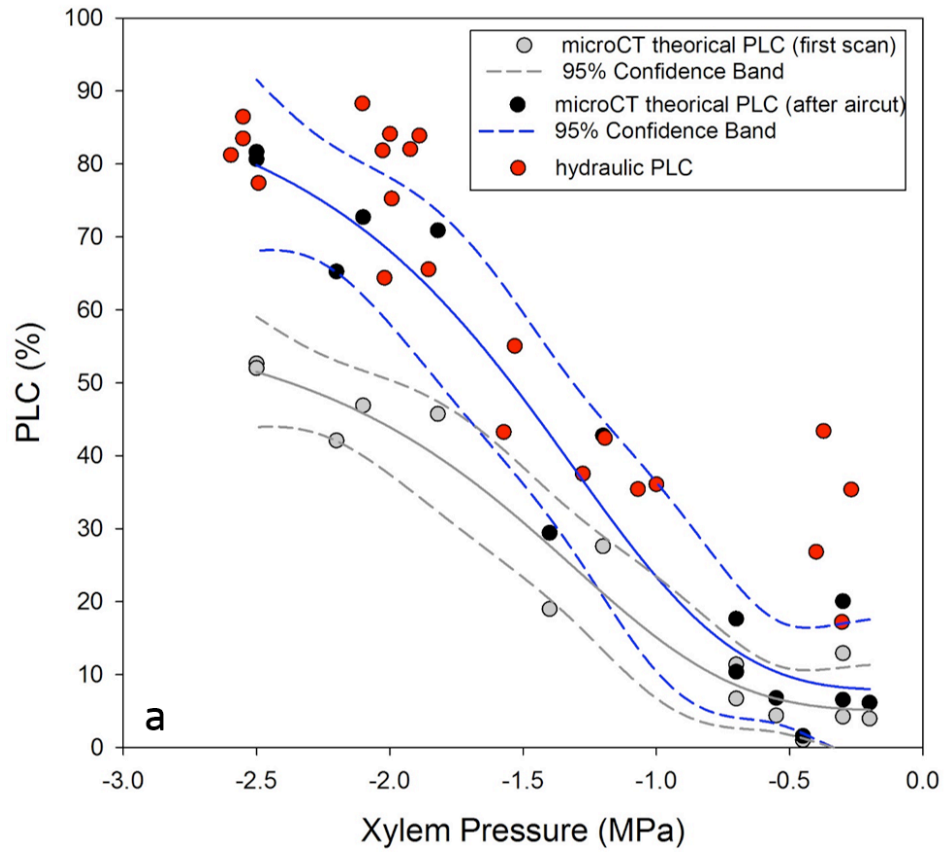
674

675



676

677 Fig. 1

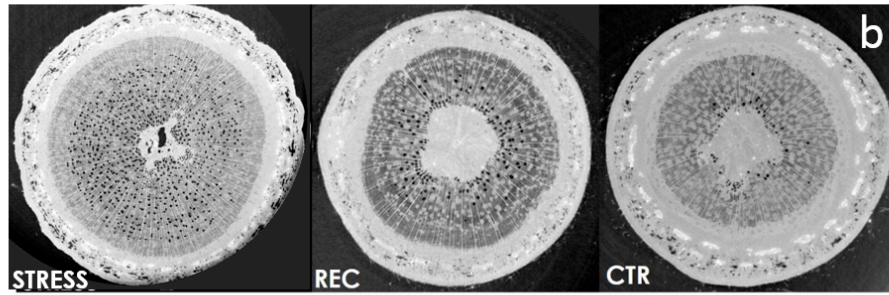
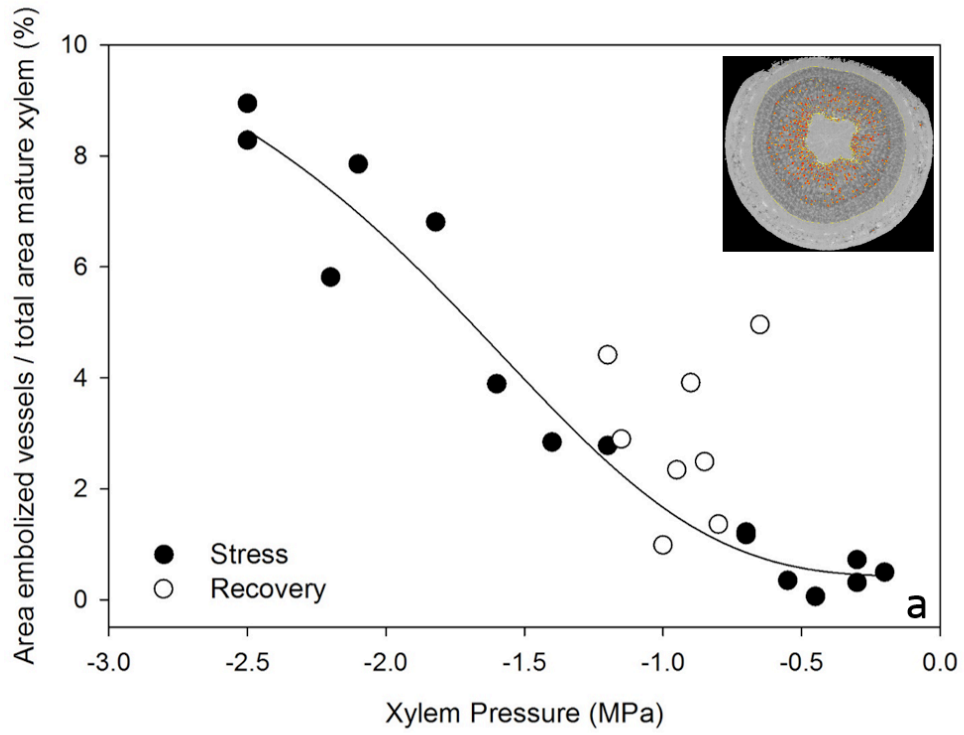


678

679 Fig. 2

680

681

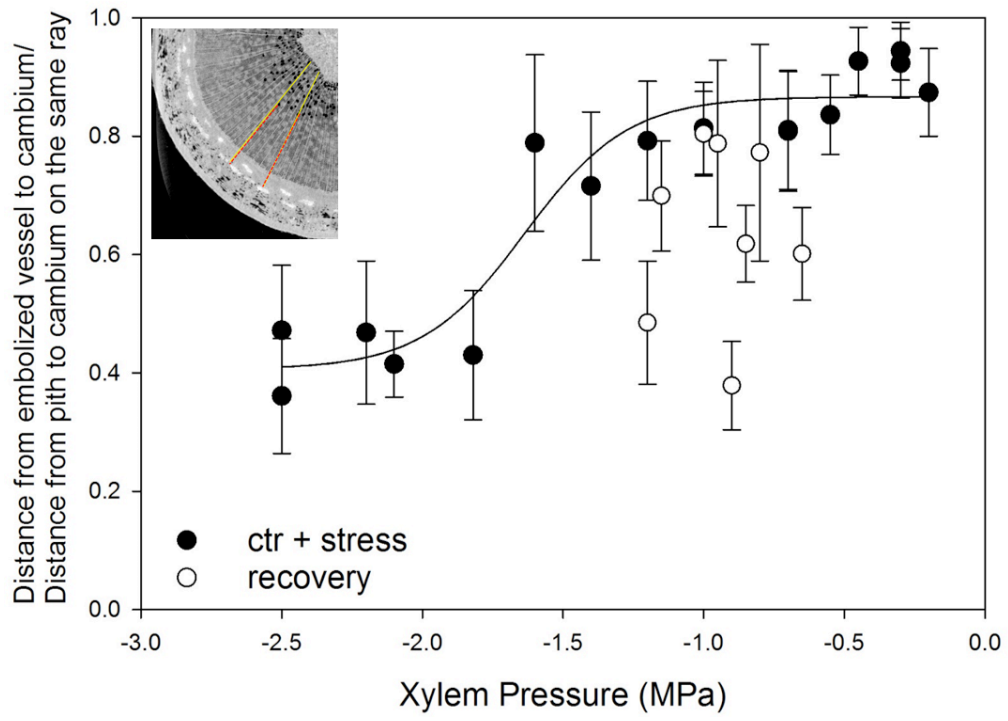


682

683 Fig. 3

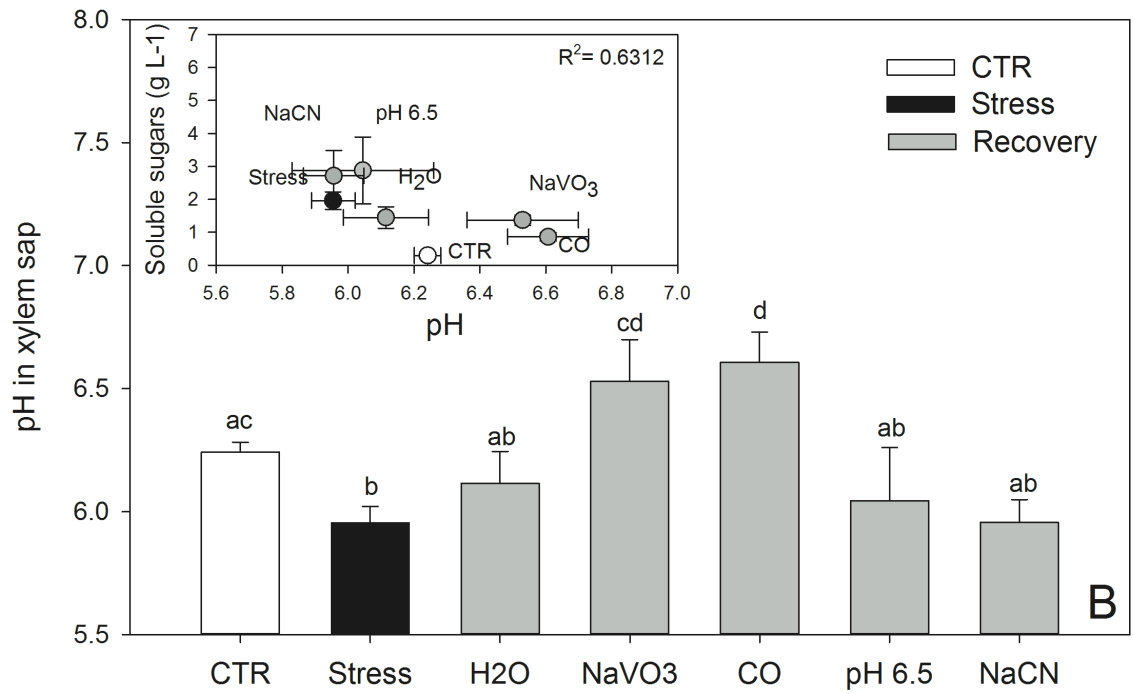
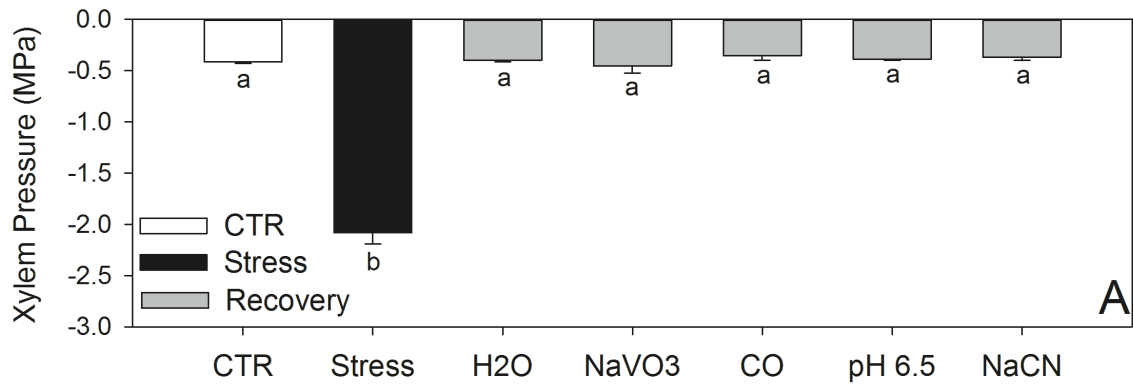
684

685



686

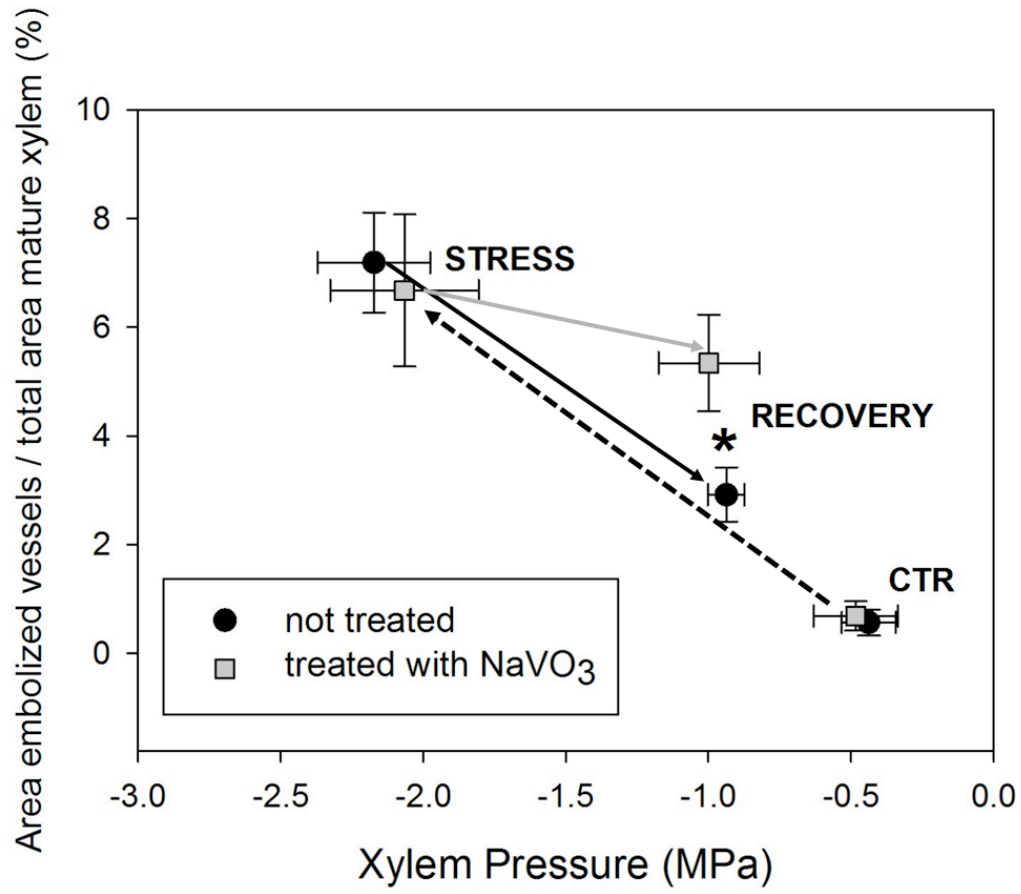
687 Fig. 4



688

689 Fig. 5

690



691

692 Fig. 6

693